JACS
JOURNAL OF THE AMERICAN CHEMICAL SOCIETY
Article
pubs.acs.org/JACS

Interplay of Charge State, Lability, and Magnetism in the Molecule-like $Au_{25}(SR)_{18}$ Cluster

Sabrina Antonello,[‡] Neranjan V. Perera,[§] Marco Ruzzi,[‡] José A. Gascón,*[,§] and Flavio Maran*[,‡,§]

[‡]Department of Chemistry, University of Padova, via Marzolo 1, 35131 Padova, Italy
[§]Department of Chemistry, University of Connecticut, 55 North Eagleville Road, Storrs, Connecticut 06269 United States

Supporting Information

ABSTRACT: $Au_{25}(SR)_{18}$ (R = $-CH_2-CH_2-Ph$) is a molecule-like nanocluster displaying distinct electrochemical and optical features. Although it is often taken as an example of a particularly well-understood cluster, very recent literature has provided a quite unclear or even a controversial description of its properties. We prepared monodisperse $Au_{25}(SR)_{18}^0$ and studied by cyclic voltammetry, under particularly controlled conditions, the kinetics of its reduction or oxidation to a series of charge states, −2, −1, +1, +2, and +3. For each electrode process, we determined the standard heterogeneous electron-transfer (ET) rate constants and the reorganization energies. The latter points to a relatively large inner reorganization. Reduction to form $Au_{25}(SR)_{18}^{2-}$ and oxidation to form $Au_{25}(SR)_{18}^{2+}$ and $Au_{25}(SR)_{18}^{3+}$ are chemically irreversible. The corresponding decay rate constants and lifetimes are incompatible with interpretations of very recent literature reports. The problem of how ET affects the Au_{25} magnetism was addressed by comparing the continuous-wave electron paramagnetic resonance (cw-EPR) behaviors of radical $Au_{25}(SR)_{18}^0$ and its oxidation product, $Au_{25}(SR)_{18}^+$. As opposed to recent experimental and computational results, our study provides compelling evidence that the latter is a diamagnetic species. The DFT-computed optical absorption spectra and density of states of the −1, 0, and +1 charge states nicely reproduced the experimentally estimated dependence of the HOMO−LUMO energy gap on the actual charge carried by the cluster. The conclusions about the magnetism of the 0 and +1 charge states were also reproduced, stressing that the three HOMOs are not virtually degenerate as routinely assumed: In particular, the splitting of the HOMO manifold in the cation species is severe, suggesting that the usefulness of the superatom interpretation is limited. The electrochemical, EPR, and computational results thus provide a self-consistent picture of the properties of $Au_{25}(SR)_{18}$ as a function of its charge state and may furnish a methodology blueprint for understanding the redox and magnetic behaviors of similar molecule-like gold nanoclusters.

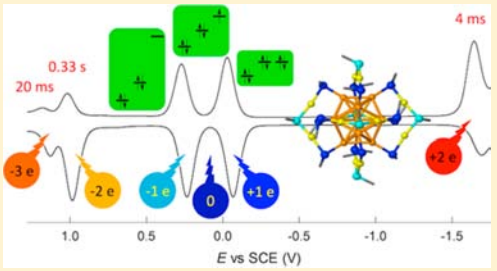

INTRODUCTION

$Au_{25}(SR)_{18}$ (R = phenylethanethiolate) is the most studied and stable form among gold clusters displaying molecule-like behavior.[1] $Au_{25}(SR)_{18}$ has a core composed by an Au_{13} centered icosahedron surrounded by six $Au_2(SR)_3$ units in which the 12 Au atoms are stellated on 12 faces of the core (Figure 1).[2] The 18 ligands thus split into a group of 12 "inner" ligands, with sulfur bonded to one stellated Au atom and one core Au atom, and a second group of 6 "outer" ligands, with sulfur clamped by two stellated Au atoms. In its native form, i.e., as prepared, $Au_{25}(SR)_{18}$ is negatively charged and diamagnetic.[2a,b,3] On the other hand, under mild oxidizing conditions, such as in the presence of oxygen, or upon addition of a suitable oxidant, $Au_{25}(SR)_{18}^-$ undergoes oxidation to form the very stable $Au_{25}(SR)_{18}^0$ species.[2c,4] The latter is a paramagnetic species displaying characteristic nuclear magnetic resonance (NMR)[4] and electron paramagnetic resonance (EPR)[5] behaviors. Density functional theory (DFT) calculations on simple models of these clusters, $Au_{25}(SH)_{18}$ and $Au_{25}(SMe)_{18}$, point to three almost degenerate highest occupied molecular orbitals (HOMOs).[6] A DFT study of $Au_{25}(SR)_{18}^-$ with *para*-substituted thiophenolate ligands pointed to one of the HOMOs as slightly higher in energy than the other two (0.12−0.13 eV).[7]

As we said, $Au_{25}(SR)_{18}^0$ is paramagnetic, and its NMR behavior is thus substantially different from that of $Au_{25}(SR)_{18}^-$. Therefore, on the basis of the near degeneracy of the HOMOs mentioned above, further oxidation of the cluster to its +1 charge state should generate another paramagnetic (diradical) species. However, according to the results that we obtained through controlled oxidation of $Au_{25}(SR)_{18}^0$ with the dissociative electron-transfer (ET)-type acceptor[8] bis-(pentafluorobenzoyl) peroxide,[9] the resulting $Au_{25}(SR)_{18}^+$ species shows an NMR behavior that closely resembles that of $Au_{25}(SR)_{18}^-$, which indicates that $Au_{25}(SR)_{18}^+$ is, in fact, another diamagnetic species. A similar conclusion was later reached by using a different oxidant.[10] The charge-dependent magnetism scenario, however, becomes more complicated owing to the very recent and intriguing observation of some EPR spectral behavior attributed to paramagnetism of $Au_{25}(SR)_{18}^+$, obtained from $Au_{25}(SR)_{18}^0$ by following the

Received: July 31, 2013
Published: September 17, 2013

   dx.doi.org/10.1021/ja407887d | J. Am. Chem. Soc. 2013, 135, 15585−15594

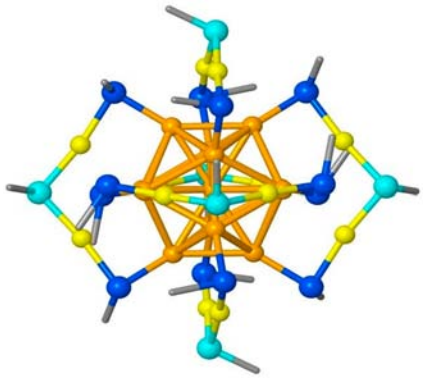

Figure 1. Structure of $Au_{25}[S(CH_2)_2Ph]_{18}$: core Au atoms (dark yellow), stellated Au atoms (light yellow), inner-ligand S atoms (blue), outer-ligand S atoms (light blue). For clarity, the R groups have been omitted.

aforementioned peroxide-induced oxidation approach.[11] In other words, there are opposite views on the magnetic state of the +1 species. Concerning the UV−vis absorption behaviors of the clusters with −1, 0, and +1 charge states, the corresponding spectra roughly display similar patterns but also show some different features (peaks and shoulders, and their position) and absorption onsets.[4,9,10] Based on our own experimental results, the HOMO−LUMO gap (LUMO = lowest unoccupied molecular orbital) of $Au_{25}(SR)_{18}^0$ and $Au_{25}(SR)_{18}^+$ is larger by ∼0.13 and 0.20 eV, respectively,[4] than that of $Au_{25}(SR)_{18}^-$, 1.33 eV.[12]

Besides energy and magnetism differences, a change of the charge state also affects the lability of the cluster, an issue that, similarly to any other molecular species, should never be underestimated in studying monolayer protected clusters. $Au_{25}(SR)_{18}^0$ is a fully stable species, $Au_{25}(SR)_{18}^-$ is stable under anaerobic conditions, and $Au_{25}(SR)_{18}^+$ is stable for several hours (we previously observed that overnight some transformation of the NMR signal occurs).[4] In the time scale of cyclic voltammetry (CV) or differential pulse voltammetry (DPV), the corresponding redox peaks are thus chemically reversible. The $Au_{25}(SR)_{18}^0/Au_{25}(SR)_{18}^-$ and the $Au_{25}(SR)_{18}^+/Au_{25}(SR)_{18}^0$ redox couples (their formal potential, $E°$, values are −0.077 and 0.226 V vs SCE, respectively, in dichloromethane, DCM, containing 0.1 M Bu_4NPF_6, TBAH)[13] can thus be used as stable ET mediators in redox-catalysis experiments.[9] Important lability differences, however, arise for higher charge states. Reduction to $Au_{25}(SR)_{18}^{2-}$ is associated with chemical processes that make the CV peak become irreversible. Reversibility can be attained only at high potential scan rate (v) values and/or low temperatures. Analysis showed that irreversibility is associated with a cascade sequence of intramolecular dissociative ET reactions[8] with release of thiolated-type species.[13] Besides the already mentioned redox processes, scanning the potential toward more positive potentials than those of the $Au_{25}(SR)_{18}^+/Au_{25}(SR)_{18}^0$ redox couple reveals the presence of further oxidation peaks. These peaks are chemically irreversible but become reversible at low temperatures, as originally reported by Murray and his co-workers.[12] It is, therefore, surprising that an UV−vis spectrum attributed to $Au_{25}(SR)_{18}^{2+}$, prepared by (slow) aerobic stepwise-oxidation of $Au_{25}(SR)_{18}^-$, could be obtained.[14]

ET reactions are accompanied by reorganization of the molecular species involved and the surrounding medium.[15] The former, inner reorganization, is due to molecular deformation of relevant bond lengths and angles of the reacting system on its way to the ET product state. Although a comparison between the structures of the anionic and neutral forms[2] shows that the former is slightly distorted because of its interaction with the counterion, tetra-*n*-octylammonium, it is quite unlikely that a similar interaction could be present in solution, particularly under electrochemical conditions where ET occurs in the presence of a large excess of supporting electrolyte (generally, a tetrabutylammonium salt). Marcus analysis[15] of the kinetics of oxidation of $Au_{25}(SR)_{18}^-$ showed that this process is indeed endowed by significant inner reorganization, no matter whether ET is carried out electrochemically,[13] studied by the NMR electron self-exchange approach,[16] or characterized in the solid state.[17] Raman results point to a Au−S bond length change upon oxidation as the main contribution to inner reorganization.[16] These results thus indicate that the HOMO and LUMO are not simply delocalized over the Au_{13} core, as implied in calculations.[2b,6a,b] Finally, we note that the nature of the actual species involved in individual ET steps and the time scale in which these events take place are elements of crucial importance that cannot be neglected in mechanistic analyses of ET applications of Au_{25} clusters, such as when used in electrogenerated chemiluminescence experiments.[18]

The above scenario thus shows that a series of intriguing results and corresponding interpretations do not harmonize toward a self-consistent and uniform picture. Here we describe results based on an in-depth experimental and computational study that provides important insights into these and related issues, leading to clarify the nature and stability of a series of $Au_{25}(SR)_{18}$ species. By using monodisperse $Au_{25}(SR)_{18}^0$ samples yielding faradic curves void of contaminations and taking advantage of an electrode/solvent/electrolyte system furnishing ideal background curves, we studied the electrode kinetics and determined the reorganization energies of $Au_{25}(SR)_{18}^z$ as a function of the charge z, where z = −2, −1, 0, +1, +2, and +3. CV also allowed us to assess the lifetime of particularly labile Au_{25} species, i.e., with two or more charges. We then used low- and high-temperature continuous wave EPR (cw-EPR) experiments to gain insights into the magnetism of $Au_{25}(SR)_{18}^+$ and possible energy differences among the first HOMOs. Finally, by DFT calculations we obtained insightful information into how the frontier orbitals evolve across different oxidation states, which were analyzed by taking into account the experimental inputs.

EXPERIMENTAL SECTION

Chemicals. Monodisperse $Au_{25}(SCH_2CH_2Ph)_{18}^0$ was prepared and characterized as already described.[4] The clusters were kept at 4 °C, in the dark, and their quality always checked before use by UV−vis and ^{1}H NMR spectroscopies. The UV−vis spectra were recorded with a Thermo Scientific Evolution 60S spectrophotometer, and the ^{1}H NMR spectra were obtained in toluene-d_8 (99.6%, d_8, Aldrich) using a Bruker model Avance DRX-400 MHz spectrometer. Dichloromethane (VWR, 99.8%) was freshly distilled over CaH_2. Tetra-*n*-butylammonium hexafluorophosphate (Fluka, 99%) was recrystallized from ethanol. Ferrocene (Carlo Erba, RPE) was recrystallized by sublimation using a coldfinger. Bis(pentafluorobenzoyl) peroxide, which is a moderately stable peroxide (it decomposes on standing at room temperature for some days; no explosions, however, were experienced during or after its preparation), was prepared as already described,[4] stored at 4 °C in the dark, and used within days.

Electrochemistry. The working electrode was a 0.55 mm radius glassy carbon (GC) disk prepared as already described.[19] The

dx.doi.org/10.1021/ja407887d | J. Am. Chem. Soc. 2013, 135, 15585−15594

electrode was initially polished using silicon carbide papers (500, 1000, 2400, and 4000), diamond pastes (Struers: 3, 1, and 0.25 μm), alumina (BDH: 0.075 and 0.015 μm) and then stored in ethanol. Before use, the electrode was further polished with 0.015 μm alumina, ultrasonically rinsed with ethanol for 5 min, washed with acetone, and carefully dried with a cold air stream. This type of electrode and procedure ensures formation of a very reproducible surface particularly suitable for ET studies.[20] Once inserted into the electrochemical cell, the GC electrode was activated in the background solution, DCM containing 0.1 M TBAH, by means of several voltammetric cycles at a scan rate of 0.5 V s^{-1} between the anodic and the cathodic potential limits of concern. The electrode's electrochemical area, 9.64×10^{-3} cm^2, was determined with reference to low scan rate voltammetric oxidation of ferrocene in *N*,*N*-dimethylformamide/0.1 M *n*-Bu_4NClO_4, in which ferrocene has a diffusion coefficient of 1.13×10^{-5} cm^2 s^{-1}. A Pt wire was the counter electrode and an Ag wire, kept in a tube filled with the same electrolyte solution but separated from the main compartment by a Vycor frit, served as a quasi-reference electrode. At the end of each experiment, the potential of the Ag quasi-reference electrode was calibrated against the ferricenium/ferrocene (Fc^+/Fc) redox couple (in the same solvent/electrolyte system, E°_{Fc/Fc^+} = 0.460 V against the KCl saturated calomel electrode, SCE). Potential values are reported against SCE.

For the electrode kinetics experiments we used an EG&G-PARC 173/179 potentiostat-digital coulometer, an EG&G-PARC 175 universal programmer, and a Nicolet 3091 12-bit resolution digital oscilloscope. Some measurements, such as to determine the equilibrium potential, to double-check some heterogeneous kinetics results, and for the DPV experiments, we used a CHI 660c electrochemical workstation. To minimize the ohmic drop between the working and the reference electrodes, careful feedback correction was employed. Our procedures were double checked by carrying out specific test experiments under the same and further experimental conditions. Standard heterogeneous rate-constant results for ferrocene oxidation were 2.2 (acetonitrile/0.1 M *n*-Bu_4NClO_4), 0.39 (*N*,*N*-dimethylformamide/0.1 M *n*-Bu_4NClO_4), and 0.40 cm s^{-1} (*N*,*N*-dimethylformamide/0.1 M *n*-Bu_4NPF_6), in line with results from other electrochemical laboratories.[21] The experiments were conducted under an Ar atmosphere in a glass cell thermostatted at 25 °C. The quality of the electrode and solvent/electrolyte system was first checked in the background solution by CV. The digital faradic CV curves were corrected by subtracting the corresponding curves (same potential range and scan rate) previously obtained in the absence of $Au_{25}(SR)_{18}$. The CV analysis was carried out using the Nicholson method[22] and digital simulations, using the DigiSim 3.03 package (stepsize = 1 mV, exponential expansion factor = 0.5). For the DPV experiments we used peak amplitude of 50 mV, pulse width of 0.05 s, 2 mV increment per cycle, and pulse period of 0.1 s.

Computational Methods. Optimization and single point energy calculations of different charge states were carried out using density functional theory (DFT) as implemented in TURBOMOLE.[23] We employed the S-VWN functional and def2-TZVP basis set for C, S, and H. For Au atoms, def2-ecp was used, which is an effective core potential that includes scalar relativistic effects. Optical absorption spectra were calculated using time-dependent DFT theory (TDDFT) under the resolution of identity (RI) approximation.

Electron Paramagnetic Resonance. For cw-EPR experiments at T < 50 K, we used 2 mM solutions of $Au_{25}(SR)_{18}^0$ or $Au_{25}(SR)_{18}^+$ in DCM. The solution containing $Au_{25}(SR)_{18}^+$ was freshly prepared by oxidation of $Au_{25}(SR)_{18}^0$ with bis(pentafluorobenzoyl) peroxide.[4,9] The solutions were introduced into 2.8 mm i.d. quartz tubes, degassed by several freeze–pump–thaw cycles and sealed off under vacuum (5×10^{-5} Torr). The samples were then rapidly cooled down to 77 K, and the EPR measurements were carried out at 6–50 K within 4 h after preparation of the solutions. Further cw-EPR experiments were carried out in DCM solution, at T = 260 K, and in frozen glassy matrix, at 120 K. We used freshly prepared samples of 1 mM $Au_{25}(SR)_{18}^0$, taken as a reference, $Au_{25}(SR)_{18}^+$, and a third solution in which $Au_{25}(SR)_{18}^0$ was treated with 2 equiv (1 molar equiv) of peroxide. The solutions were still degassed and sealed under vacuum but using 0.8 mm i.d. quartz tube. After sealing, the samples were cooled down and then analyzed by EPR at the appropriate temperature within 20 min from preparation.

X band cw-EPR spectra were recorded with a Bruker ER200D spectrometer equipped with a standard cylindrical TE011 cavity. The temperature was controlled by a helium flow cryostat system equipped with a variable-temperature controller unit (Oxford ITC-4). All experimental data were collected under nonsaturating microwave conditions (microwave power: P_{MW} = 250 μW or lower). A modulation frequency of 100 kHz and amplitude (peak-to-peak) of 5 G were used for all spectra. Simulation of EPR spectra were carried out using Matlab routines from EasySpin toolbox.[24] To estimate the spin concentration in the samples, we used a comparison method based on recording spectra in the presence of an external standard reference and then normalizing them relative to the standard reference EPR signal. The ratio of double-integrated EPR spectra (areas under absorption EPR spectra), recorded for the pristine and oxidized clusters, provides an estimate of the relative spin concentration of the samples.

RESULTS AND DISCUSSION

Electrochemistry. The heterogeneous ET behavior of $Au_{25}(SR)_{18}$ was studied on a GC disk electrode in DCM/0.1 M TBAH. The temperature was controlled at 25 °C, although for specific kinetic studies, lower temperatures were also used. For all experiments, the starting cluster was the $Au_{25}(SR)_{18}^0$ radical. Compared to $Au_{25}(SR)_{18}^-$, for which the equilibrium potential (potential at which no current flows) is negative to the $Au_{25}(SR)_{18}^-$ oxidation peak,[12] the corresponding potential for $Au_{25}(SR)_{18}^0$ rests at a more positive value, +0.088 V,[9] in between the peak of the $Au_{25}(SR)_{18}^0/Au_{25}(SR)_{18}^-$ and $Au_{25}(SR)_{18}^+/Au_{25}(SR)_{18}^0$ redox couples. We thus had the opportunity of studying the heterogeneous ET kinetics of these redox processes by initiating the potential scan in either the positive or negative going direction (Figure 2), a quite uncommon situation indeed in molecular electrochemistry. At low υ values and for both the first oxidation and reduction peaks (hereafter defined as O1 and R1, respectively, to stress the final charge state), the separation between the anodic and the cathodic peak potentials (ΔE_p) exhibits the reversible value of ~59 mV.[25] The diffusion coefficient (D) of $Au_{25}(SR)_{18}$, 4.0×10^{-6} cm^2 s^{-1},[26] was calculated from low scan-rate peak-current (i_p) measurements.[25] It is worth stressing that we used extremely pure materials and very controlled electrochemical conditions leading to immaculate CV patterns. As a matter of fact, it is particularly rewarding to note that on the basis of the Stokes–Einstein equation ($D = k_BT/6\pi\eta r$, where k_B is the Boltzmann constant, η is the solvent viscosity, and r is the molecular radius), the above experimental D value corresponds to a radius r of 13.2 Å, i.e., exactly the same value calculated from the gold core (5 Å)[2a] plus the van der Waals thickness of the monolayer, 8.2 Å.[27]

For sufficiently high υ values and for both peaks, ΔE_p increases, as illustrated in Figure 2. This indicates that as the time scale of the experiment decreases, the heterogeneous ET starts becoming quasi-reversible. The standard heterogeneous ET rate constant (k°) is the ET rate constant measured at an applied potential (E) corresponding to E°.[28] The smaller k°, the larger ΔE_p. k° was thus obtained by studying the υ dependence of ΔE_p, according to the Nicholson method.[22] For both O1 and R1 processes, the plot of ΔE_p vs log $\upsilon^{1/2}$ shows an excellent fit to the Nicholson theoretical curve (Figure 3) in the whole scan rate range investigated, 0.1–50 V s^{-1}. Digital simulation of the experimental CV curves confirmed both k° determinations.

dx.doi.org/10.1021/ja407887d | J. Am. Chem. Soc. 2013, 135, 15585–15594

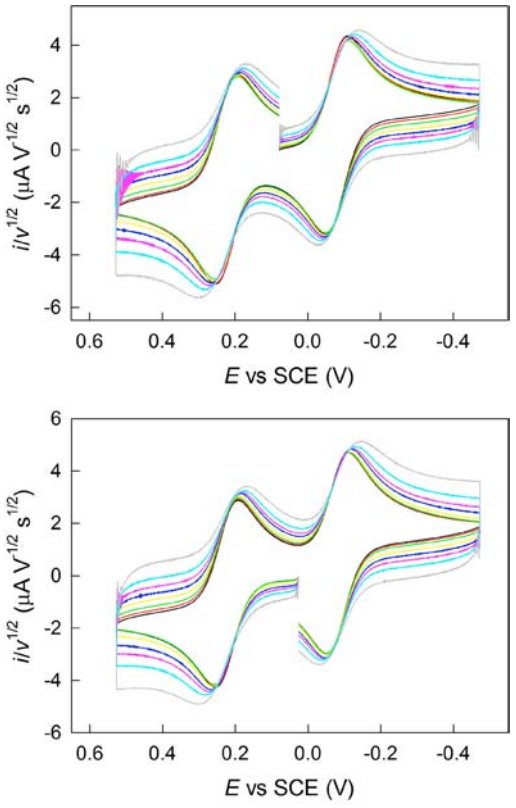

Figure 2. Cyclic voltammetry curves for the reduction of 0.91 mM $Au_{25}(SR)_{18}^{0}$ in DCM/0.1 M TBAH on a GC electrode. The scan rates are 0.1, 0.2, 0.5, 1, 2, 5, 10, and 20 V s^{-1}. The CV curves, normalized with respect to scan rate (i.e., $i/v^{1/2}$), can be identified based on the increasing capacitive-current component, which depends linearly on v, whereas the faradic component depends on $v^{1/2}$.[22] T = 25 °C. In the upper and lower graphs the initial scan direction is negative and positive, respectively.

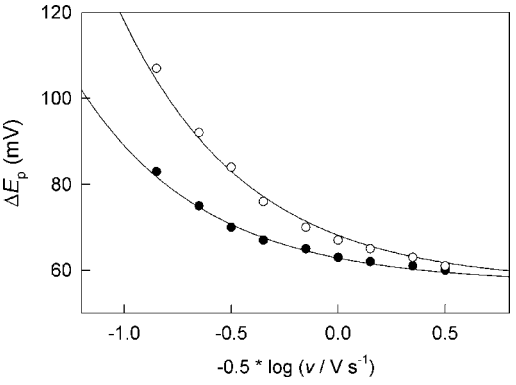

Figure 3. Scan rate dependence of the separation between the cathodic and the anodic peak potentials for the reduction (●) and oxidation (○) of 0.91 mM $Au_{25}(SR)_{18}^{0}$ in DCM/0.1 M TBAH at the GC electrode, T = 25 °C. The plots show the best fit of the data to the theoretical curve describing the competition between the diffusion and the ET steps.[22] The transfer coefficient α was set to 0.5, and the same D value was used for all charge states.

For R1 and O1 we obtained different k° values (Table 1).[29] Whereas for R1 k° is 0.16 cm s^{-1}, the value for the formation of $Au_{25}(SR)_{18}^{+}$ is 0.073 cm s^{-1}. Both values are within typical values obtained for common outer-sphere acceptors or donors.[30,31] Once corrected for the D value,[26] the R1's k° value is the same as previously obtained starting, however, from $Au_{25}(SR)_{18}^{-}$.[13] For the other redox couple, $Au_{25}(SR)_{18}^{+}$/$Au_{25}(SR)_{18}^{0}$, we carried out a second determination of its k° value, this time starting from $Au_{25}(SR)_{18}^{+}$. The latter was obtained by adding 0.5 molar equiv of bis(pentafluorobenzoyl) peroxide to a solution of $Au_{25}(SR)_{18}^{0}$. This peroxide, which undergoes a two-electron dissociative reduction[32] at very positive potentials, operates as an effective two-electron oxidant and is able to convert quantitatively the neutral $Au_{25}(SR)_{18}^{0}$ to its oxidized state.[4,9] Thus, we started the CV experiments from a new equilibrium potential, ca. 0.67 V, and scanned the potential negatively. The value of k° obtained by following this alternative procedure was exactly the same of that starting from $Au_{25}(SR)_{18}^{0}$. Therefore, for both redox couples the same k° values were obtained no matter whether the potential scan was initiated starting from $Au_{25}(SR)_{18}^{-}$, $Au_{25}(SR)_{18}^{0}$, or $Au_{25}(SR)_{18}^{+}$, which further confirms the reliability of the methodologies employed.

From the k° values and using the Eyring-type equation $k^{\circ} = Z\exp(-\Delta G_0^{\ddagger}/RT)$, the ET intrinsic barriers ($\Delta G_0^{\ddagger}$) pertaining to O1 and R1 were calculated. These and further results (see below) are collected in Table 1. $\Delta G_0^{\ddagger}$ is the activation free energy when the reaction free energy (ΔG°) is 0; it is known as the intrinsic barrier because it defines the kinetic facility of the ET reaction. $\Delta G_0^{\ddagger}$ is composed by the outer component ($\Delta G_{0,s}^{\ddagger}$), arising from the solvent reorganization associated with the charge variation, and the inner component ($\Delta G_{0,i}^{\ddagger}$), already defined. Z was calculated to be 730 cm^{-1} ($Z = (RT/2\pi M)^{1/2}$,[30] where M is the molar mass). The resulting $\Delta G_0^{\ddagger}$ values for R1 and O1 are 5.0 and 5.4 kcal mol^{-1}, respectively. $\Delta G_{0,i}^{\ddagger}$ was obtained by subtracting the solvent reorganization term from $\Delta G_0^{\ddagger}$. $\Delta G_{0,s}^{\ddagger}$ (1.2 kcal mol^{-1}) was calculated from the Hush equation,[33] $\Delta G_{0,s}^{\ddagger} = e^2(1/\varepsilon_{op} - 1/\varepsilon_s)/8r$ (where e is the charge of the electron, and ε_{op} and ε_s are the high frequency and static dielectric constants of the solvent, respectively), using the above value of r = 13.2 Å for $Au_{25}(SR)_{18}$. $\Delta G_{0,s}^{\ddagger}$ was also calculated[16] by considering only the radius of the gold core (i.e., without including the capping monolayer thickness) and ε_{op} and ε_s values obtained on the basis of the dielectric properties of the monolayer, as the actual surrounding medium. The truth probably is in between these two approaches because according to the structure[2] the Au_{25} monolayer is not as tight as in self-assembled monolayers on extended gold surfaces (2D SAMs)[34] and it is thus somehow permeable to exogenous molecules as supported by the solvent effect[12,13] on O1 and R1 as well as very recent homogeneous ET processes involving the same Au_{25} species.[9] Incidentally, however, such an alternative approach yields an almost identical value of $\Delta G_{0,s}^{\ddagger}$, 1.3 kcal mol^{-1}. To conclude, our experimental results show that a larger inner intrinsic barrier is involved in the formation of the nanoparticle monocation (peak O1) compared to formation of the monoanion (peak R1). Since the reorganization energy is four times larger than the intrinsic barrier ($\lambda = 4\Delta G_0^{\ddagger}$),[15] we conclude that the inner reorganization component (λ_i) of O1 is larger than that of R1 by 1.6 kcal mol^{-1}.

Let us now consider the other redox states. By scanning the potential negatively of R1 or positively of O1, further peaks are detected. For clarity, these peaks are compared in Figure 4 in terms of the DPV behavior of $Au_{25}(SR)_{18}^{0}$. The corresponding background curves are displayed to evidence better the faradic peaks. Concerning R2, we previously reported that the dianion is not stable in the time scale of DPV and CV experiments, at least at room temperature.[13] The electroreduction mechanism proceeds by a sequence of stepwise dissociative ET steps

dx.doi.org/10.1021/ja407887d | J. Am. Chem. Soc. 2013, 135, 15585−15594

Table 1. Electrochemical Parameters, Standard Rate Constants, Decay Rate Constants, Intrinsic Barriers ($\Delta G_0^{\ddagger}$), and Inner Intrinsic Barriers ($\Delta G_{0,i}^{\ddagger}$) for the Oxidation and the Reduction of $Au_{25}(SR)_{18}$ Clusters on GC in DCM at 25 °C

peak (charge states)	E° (V)	k° (cm s^{-1})	$\Delta G_0^{\ddagger}$ (kcal mol^{-1})	$\Delta G_{0,i}^{\ddagger}$ (kcal mol^{-1})	k_d (s^{-1})
R2 (−1/−2)	−1.72[a]	0.030[a,b]	6.0	4.8	250[c]
R1 (0/−1)	−0.077[d]	0.16[a,e,f]	5.0	3.8	stable
O1 (+1/0)	0.226[d]	0.073[a,e,f]	5.4	4.2	stable (hours)
O2 (+2/+1)	0.96$_s$[a]	0.070[a,g]	5.5	4.3	3
O3 (+3/+2)	1.16[a]	0.11[a,g]	5.2	4.0	50

[a]Digital simulation. [b]Uncertainty is 25%. [c]From ref 13. [d]Formal potential is obtained as the average of the reduction and the oxidation peak potentials. [e]ΔE_p method. [f]Uncertainty is 15%. [g]Uncertainty is 20%.

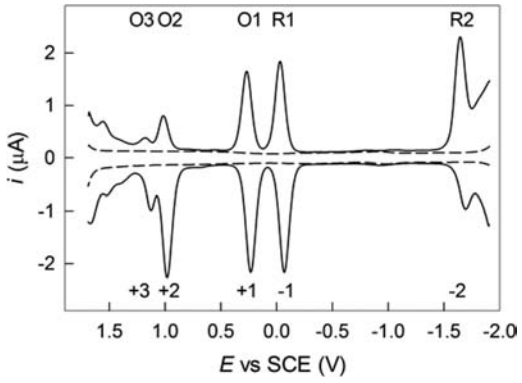

Figure 4. DPV behavior of 0.70 mM $Au_{25}(SR)_{18}^0$ in DCM/0.1 M TBAH on a GC electrode. The dashed lines show the corresponding background contribution. The peaks have been labeled (top) and the charge state indicated (bottom), T = 25 °C.

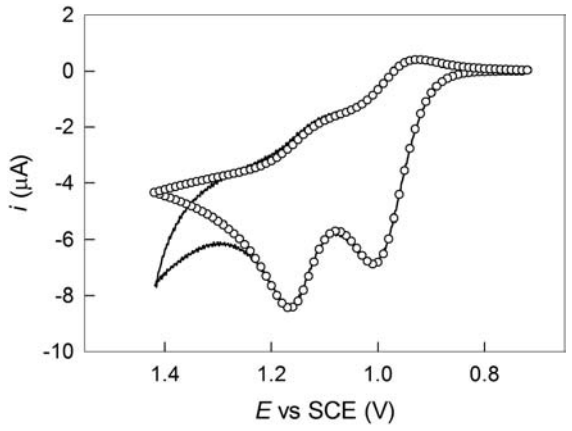

Figure 5. Background-subtracted CV for the oxidation of $Au_{25}(SR)_{18}^+$ in DCM/0.1 M TBAH on a GC electrode at 25 °C. The curve was obtained at 1 V s^{-1} starting from a 1.04 mM solution of $Au_{25}(SR)_{18}^0$ that was previously polarized at 0.72 V for 20 s. The open circles show the corresponding, optimized digitally simulated curve.

affecting the monolayer integrity of the cluster and characterized by similar formal potentials. For this peak, the ratio $i_p/v^{1/2}$ increases as v decreases (Figure S1), which implies that the number of electron per molecule (n) also increases significantly (at 0.1 V s^{-1}, $n \sim 3.5$). By digital simulation of the CV curves obtained at various scan rates, we could estimate a decay rate constant (k_d) of 250 s^{-1} and thus a lifetime of 4 ms.

CV analysis of the process leading to $Au_{25}(SR)_{18}^{2+}$ shows that, at 0.1 V s^{-1}, the O2 peak is partially reversible. By increasing v, the peak becomes chemically reversible, and then, at higher v values, the anodic peak potential (E_p) starts shifting toward more positive values; at the same time, the current function ($i_p/v^{1/2}$) undergoes a small decrease (Figure S2). The overall behavior is thus consistent with a one-electron oxidation followed by a chemical reaction (EC mechanism) and becomes electrochemically quasi-reversible at moderate v values. The analysis of the O2 peak was carried out by starting the voltammetric scan from either the equilibrium potential of $Au_{25}(SR)_{18}^0$ or an E value, 0.72 V, more positive than that of the O1 peak; this potential was held for 20 s, to accumulate $Au_{25}(SR)_{18}^+$ at the electrode surface, and then the CV scan was started. The curves on which digital simulation was carried out (such as that in Figure 5) were obtained by subtracting the background contribution, using CVs previously acquired under the same conditions. Figure 5 also shows the subsequent oxidation step (peak O3). An EC mechanism was used to simulate the CVs of both O2 and O3 processes.

In this regard, it is worth stressing that at O2 we do not have the same cascade stepwise dissociative ET mechanism[8] occurring at R2.[13] This is because of the following observations. High scan-rate measurements and low-temperature studies (see below) show that O3 truly corresponds to formation of $Au_{25}(SR)_{18}^{3+}$. In other words, peak O3 is not due to an oxidizable species formed in some fragmentation process occurring at O2. On the other hand, the fact that the height of peak O3 inversely depends on the efficiency of the chemical reaction associated with peak O2 implies that such reaction subtracts $Au_{25}(SR)_{18}^{2+}$ from further oxidation at O3. Because the electroactive center is the gold core itself and considering the specific aprotic and unreactive solvent employed, the voltammetric behavior thus points to the occurrence of a cleavage reaction in which the leaving group does not carry away the extra charge, as otherwise a gold cluster with virtually the same oxidation potential of $Au_{25}(SR)_{18}^+$ would form (analogously to what happens at R2). The gold containing fragment, in turn, cannot be a "simple" Au_{25} cluster species because it would have an oxidation potential (at O3) similar to that of $Au_{25}(SR)_{18}^{2+}$ itself. A probable hypothesis is thus that the fragmentation reaction also removes gold atoms from $Au_{25}(SR)_{18}^{2+}$, thereby yielding a smaller, and thus more difficult to oxidize, cluster.

Simulation of CV curves such as that in Figure 5 requires, for both redox processes, optimization of thermodynamic and kinetic parameters, namely E°, D, k°, α (transfer coefficient), and k_d values (details are provided in the Supporting Information (SI)), and the relevant data are gathered in Table 1. The results were obtained by simulation of the voltammetric curves obtained at 25 °C. As a further check of the rate constant values, however, we also studied processes O2 and O3 as a function of temperature. As already observed in pioneer work by Murray and co-workers,[12] lowering the

dx.doi.org/10.1021/ja407887d | J. Am. Chem. Soc. 2013, 135, 15585−15594

temperature makes the O2 and O3 peaks chemically reversible (Figure S3): here we carried out a quantitative analysis, as we previously did for R2.[13] In the temperature range from −41 to −1 °C, reversible CVs could be obtained for a sufficient number of scan rates to allow the estimation of the k° values of O2 and O3 from the ΔE_p scan rate dependence. From the corresponding Arrhenius plots, we extrapolated the two k° values to 25 °C and then used them as known parameters in the simulation of the CV curves to obtain the two k_d values. The k° and k_d values were the same, within error, as those calculated directly at 25 °C.

Albeit slightly larger than the intrinsic barrier of R1, the $\Delta G_0^{\ddagger}$ values of R2, O1, O2, and O3 are still similar to those pertaining to the reduction or oxidation of delocalized redox molecules, such as those commonly employed as one-electron mediators in homogeneous redox-catalysis experiments carried out in organic solvents. For these molecules, ∼80% of $\Delta G_0^{\ddagger}$ is ascribed to solvent reorganization.[30,31] Because of its relatively large radius, however, the $\Delta G_{0,s}^{\ddagger}$ of $Au_{25}(SR)_{18}$ species is particularly small,[32] and thus subtraction of this term from $\Delta G_0^{\ddagger}$ shows that for all redox couples of the $Au_{25}(SR)_{18}$ system $\Delta G_{0,i}^{\ddagger}$ is the major component, amounting to 76−80% of $\Delta G_0^{\ddagger}$ (Table 1).

Concerning the lifetime of the various oxidation states, the order is $Au_{25}(SR)_{18}^{2-}$ (4 ms) < $Au_{25}(SR)_{18}^{3+}$ (20 ms) < $Au_{25}(SR)_{18}^{2+}$ (0.33 s). This shows that as long as the time scale of the experiment is longer than these lifetimes, there is no chance of accumulating these species for, say, UV−vis[14] or ECL experiments.[18] On the other hand, within shorter time windows one can efficiently use these charge states for, e.g., homogeneous redox catalysis as we previously demonstrated for $Au_{25}(SR)_{18}^{2-}$ by proper selection of the ET partner.[13]

Electron Paramagnetic Resonance. To establish on a comparative basis the magnetic properties of $Au_{25}(SR)_{18}^{0}$ and $Au_{25}(SR)_{18}^{+}$ and to investigate the spin multiplicity of their fundamental states, we recorded cw-EPR spectra at 6 K. Figure 6 shows the spectra of $Au_{25}(SR)_{18}^{0}$ before and after oxidation with bis(pentafluorobenzoyl) peroxide. The spectra were obtained in frozen matrix at 6 K. The spectrum of $Au_{25}(SR)_{18}^{0}$ is typical of a distribution of randomly oriented

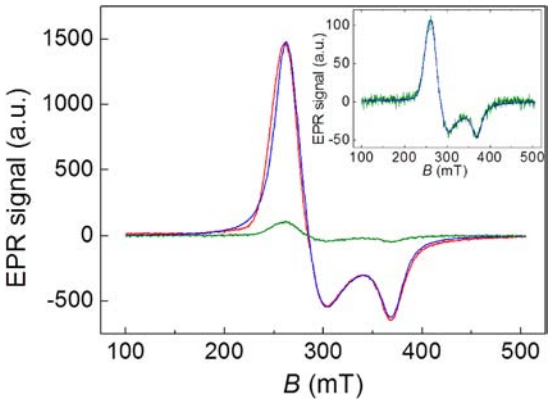

Figure 6. EPR spectra of $Au_{25}(SR)_{18}^{0}$ before (red curve) and after oxidation (green curve). Both spectra were recorded at 6 K by setting the same instrumental parameters (microwave frequency: 9.4670 GHz; microwave power: 25 μW; amplitude modulation: 0.5 mT). The blue curve shows the simulated spectrum of $Au_{25}(SR)_{18}^{0}$. The inset shows an enlarged view of the spectrum of the oxidized cluster together with the corresponding simulation (see text).

$S = 1/2$ state molecules with anisotropic g-tensor components. Recently, Zhu et al. described low-temperature cw-EPR spectra of $Au_{25}(SR)_{18}^{0}$ together with the corresponding simulation.[5] The observed significant reduction of the hyperfine isotropic coupling in the $Au_{25}(SR)_{18}^{0}$ sample was interpreted by assuming that the unpaired electron occupies an orbital sensitively lacking s-character, i.e., assuming the unpaired spin as having a negligible spin density on the Au nucleus. Main conclusion was that the observed highly delocalized spin density was consistent with a "superatom" model,[35] where most of the spin density is localized in the Au_{13} core.

Figure 6 shows that the experimental EPR spectrum of $Au_{25}(SR)_{18}^{0}$ nanoparticles (red curve) is closely reproduced by a spectral simulation (blue curve) based on previously reported anisotropic g-tensor (g = 2.56, 2.36, 1.82) and anisotropic hyperfine coupling (A = 71, 142, 50 MHz) with 13 equivalent I = 3/2 ^{197}Au nuclei.[5] We should note, however, that because of the inhomogeneous broadening caused by unresolved hyperfine components, a satisfactory simulation of the spectrum can be obtained at low temperature also by decreasing the aforementioned hyperfine coupling and increasing the g-tensor anisotropy, as already commented upon.[5] Interestingly, the use of a smaller number of equivalent Au atoms does not appreciably affect the quality of the simulation (see Figure S4 in SI), which indicates that one does not have necessarily to describe the EPR outcome on the basis of an Au_{13} core.

The oxidation of $Au_{25}(SR)_{18}^{0}$ to $Au_{25}(SR)_{18}^{+}$ was carried out using bis(pentafluorobenzoyl) peroxide. $Au_{25}(SR)_{18}^{0}$ reduces the peroxide according to a concerted dissociative ET step forming a stable carboxylate anion and the pentafluorobenzoyloxy radical; the latter also reacts by ET with another $Au_{25}(SR)_{18}^{0}$ species with formation of a second carboxylate ion.[9] We considered that even a slight excess of peroxide would have resulted in the formation of some pentafluorobenzoyloxy radical that, given the lack of sufficient co-reactant, would have decayed[36] to form products possibly affecting our cw-EPR experiments. We thus resorted to add a slight defect of peroxide. The resulting EPR spectrum shows a strong decrease in intensity. That the only signal is due to remaining $Au_{25}(SR)_{18}^{0}$ is shown in the inset of Figure 6, where the experimental curve was successfully simulated using the same parameters used for the original $Au_{25}(SR)_{18}^{0}$ sample. A relative quantification of the EPR signal intensities recorded for both the pristine and the oxidized $Au_{25}(SR)_{18}^{0}$ samples was carried out using an external standard (see Experimental Section) and normalizing the recorded spectra on the standard reference signal. A simple calculation of the double integrated intensities of the experimental spectra of the pristine and oxidized $Au_{25}(SR)_{18}^{0}$ samples (red and green spectra of Figure 6, respectively) shows that the EPR intensity of the signal recorded for the oxidized sample is ∼16 times weaker than that of $Au_{25}(SR)_{18}^{0}$. Taken together these results can be accounted for by considering a residual amount (∼6%) of nonoxidized $Au_{25}(SR)_{18}^{0}$ in the resulting $Au_{25}(SR)_{18}^{+}$ solution. The remaining $Au_{25}(SR)_{18}^{0}$ cluster thus provides sort of an internal reference for understanding the magnetic properties of $Au_{25}(SR)_{18}^{+}$. In fact, beside remaining $Au_{25}(SR)_{18}^{0}$, we did not detect any other EPR signal.

The cw-EPR spectra of the oxidation-treated $Au_{25}(SR)_{18}^{0}$ sample were recorded and simulated also for higher temperatures, in the range T = 6−50 K (Figure 7). The observed signals are still assigned to residual $Au_{25}(SR)_{18}^{0}$, as the simulations were calculated using the same g and A values

dx.doi.org/10.1021/ja407887d | J. Am. Chem. Soc. 2013, 135, 15585−15594

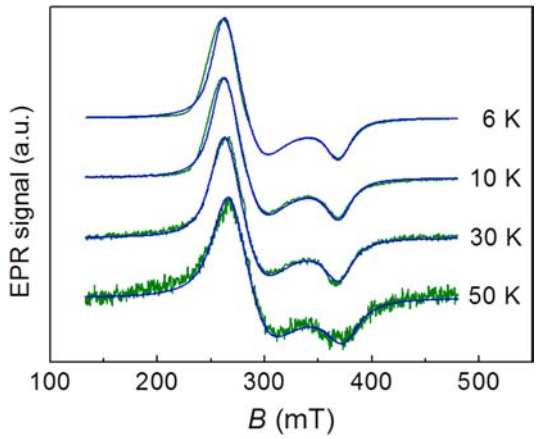

Figure 7. Experimental (green curves) and calculated (blue curves) EPR spectra of oxidized $Au_{25}(SR)_{18}^{0}$, at different temperatures. For the sake of better comparison, the curves have been shifted vertically. The experimental parameters are as in Figure 6, except for the increased microwave power (250 μW). Progressively increasing linewidths (21, 22, 25, 32 mT) and decreasing doubly integrated intensities (2×10^6, 1×10^6, 0.41×10^6, 0.18×10^6 au) were used for the simulations at 6, 10, 30, and 50 K, respectively.

employed for pristine $Au_{25}(SR)_{18}^{0}$. Except for the expected decrease of EPR intensity due to Curie law[37] and for the line broadening due to spin relaxation mechanisms, which become more efficient at higher temperatures, increasing the temperature does not significantly change the main spectral features. Linewidths and EPR intensities yielded by the simulations are given in the caption to Figure 7.[38] At higher temperatures, the EPR signals of nonoxidized $Au_{25}(SR)_{18}^{0}$ start to broaden, and the simulations of the spectra become progressively less reliable.

Figure 7 shows that no additional EPR signals are observable in the spectra, which may indicate that for $T < 50$ K, the lower energy triplet state of $Au_{25}(SR)_{18}^{+}$ is not thermally accessible (see below). In principle, however, the absence of the triplet lines in the experimental spectra of oxidized $Au_{25}(SR)_{18}^{0}$ could be explained by quick relaxation of the EPR signal. Because of the marked anisotropy of the EPR line positions arising from the spin−spin interaction between the coupled electrons, a temperature increase may cause significant line broadening in many systems with $S \geq 1$. Similar effects on linewidths may result also from a large anisotropy of the spin−orbit interaction (anisotropy of the *g*-tensor).[39] In the framework of the theory of the spin-relaxation mechanisms,[40] any dynamic process (hindered rotations, molecular reorientations, tumbling of the molecule in a viscous liquid) in and around the paramagnetic center may affect line shapes. In particular, if the rate of dynamic fluctuations of the local magnetic field at the unpaired electron(s) is sufficiently high, a dramatic broadening of EPR lines occurs. Concerning specifically triplet-state systems,[41] in nonrigid media when the anisotropic part of the zero-field splitting (ZFS) interaction is not negligible, the rapid modulation of the spin−spin interactions may lead to spin-state lifetimes so short that the averaged triplet spectrum has undetectably broad lines. Owing to modulation of the spin−orbit coupling, triplet species with a large anisotropy of the *g*-tensor may also lead to broadening effects. In the case of $Au_{25}(SR)_{18}^{+}$, however, these factors do not play a role because the very low temperatures at which we recorded the EPR spectra were such to prevent the occurrence of effects caused by fast dynamics. In other words, even for a system like $Au_{25}(SR)_{18}^{+}$, whose ZFS and anisotropies in the *g*-tensor are unknown, the EPR lines are expected to be sufficiently narrow to be confidently detected. The absence of any detectable signal assignable to the triplet state of $Au_{25}(SR)_{18}^{+}$ in the spectra of Figure 7 can thus be taken as a quite definitive evidence of the diamagnetism of such charge state.

Puzzled by the outcome of a very recent study in which some EPR signals were attributed to paramagnetism of $Au_{25}(SR)_{18}^{+}$,[11] we carried out further cw-EPR experiments at higher temperatures, both in DCM solution (at 260 K) and in frozen glassy matrix (at 120 K), using freshly prepared samples of $Au_{25}(SR)_{18}^{+}$ and even a solution in which $Au_{25}(SR)_{18}^{0}$ was treated with 2 equiv (1 molar equiv) of peroxide. In contrast to the above claim, however, in all experiments we did not detect any EPR signal either due to $Au_{25}(SR)_{18}^{+}$ clusters or other radicals. These results thus provide further evidence about the diamagnetic character of $Au_{25}(SR)_{18}^{+}$. To conclude, the EPR results and analysis show that the idea of considering $Au_{25}(SR)_{18}^{+}$ as a superatomic diradical must be dismissed.

Computational Results. A model structure of $Au_{25}(SCH_3)_{18}^{-}$ was constructed from the available $Au_{25}(SR)_{18}^{-}$ crystal structure.[2a] Ligands were slightly rotated to attain a structure with C_i point group symmetry. The states −1, 0, and +1 were prepared in that order, that is, the starting geometry for the 0 and +1 forms where the previously optimized structures of −1 and 0, respectively.

Let us first consider the transition from the −1 to the 0 charge state. The electronic structure of $Au_{25}(SCH_3)_{18}^{-}$ is characterized by a closed-shell configuration with three fully occupied $1a_u$ states (HOMOs) (in the superatom terminology, a P orbital), while the first unoccupied orbital corresponds to an a_g state (LUMO) (see orbital diagrams in Figure 8 and

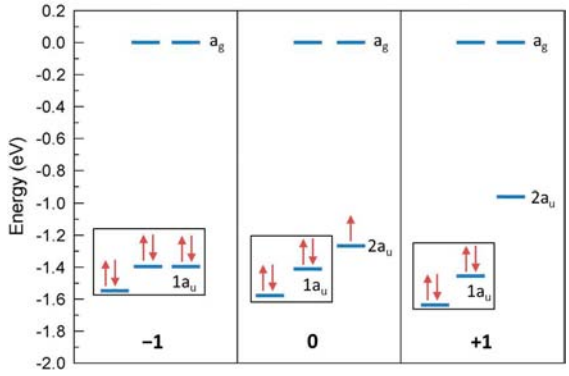

Figure 8. Orbital diagrams in $Au_{25}(SCH_3)_{18}^{z}$ ($z = -1, 0, +1$). Levels enclosed in the rectangles correspond to a single peak in the DOS plot (Figure 9).

density of states (DOS) in Figure 9). Notice that the commonly assumed triple degeneracy in the −1 state is no longer strictly applicable. This result is in agreement with Aikens's analysis of ligand effects on the frontier orbtials.[7] Nevertheless, assuming an inherited Lorentzian energy width of 0.1 eV, these three a_u levels can be regarded within a single energy manifold, herein called $1a_u$. In the −1 state, the energy separation between the $1a_u$ manifold and a_g is 1.45 eV, in good agreement with the 1.33 eV gap measured experimentally.[12] As the cluster is oxidized from −1 to 0, the $1a_u$ manifold splits, giving raise to a second distinct Lorentzian peak in the DOS (Figure 9); we call this second peak $2a_u$. In the 0 state, the gap

dx.doi.org/10.1021/ja407887d | J. Am. Chem. Soc. 2013, 135, 15585−15594

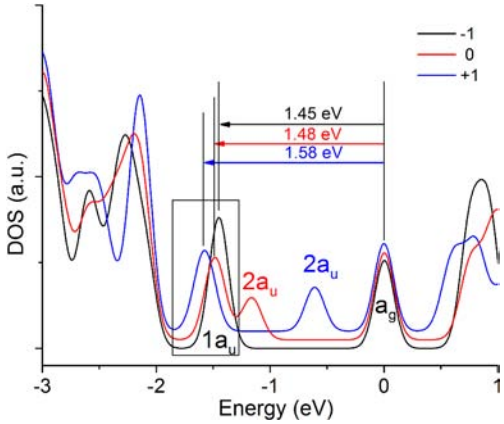

Figure 9. DOS in $Au_{25}(SCH_3)_{18}^{z}$ (z = −1, 0, +1). Curves have been slightly shifted vertically to better discern corresponding lines. The a_g state was used as the zero of energy for all charge states. DOS was constructed with 0.1 eV width Lorentzians.

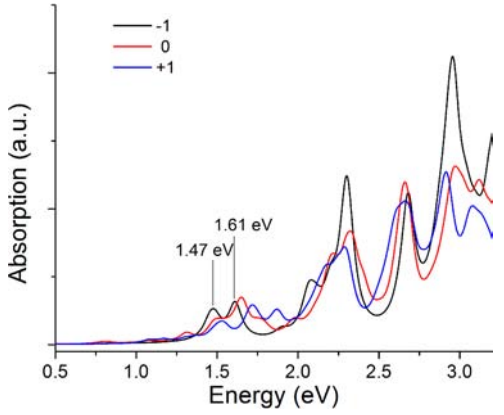

Figure 10. Calculated TDDFT absorption spectrum for $Au_{25}(SCH_3)_{18}^{z}$ (z = −1, 0, +1). Spectra were constructed with 0.1 eV width Lorentzians.

between the LUMO level and the HOMO level with the largest DOS increases by 0.03 eV. Although very small, such increase is in qualitative agreement with the experimentally measured HOMO−LUMO gap increase (0.13 eV).

A more complex situation arises for the 0 to +1 oxidation. The $2a_u$ level, which now becomes vacant in the +1 state, shifts further to higher energies. This clearly indicates that the corresponding triplet (paramagnetic) state would require a large energy promotion from $1a_u$ to $2a_u$. Thus, a paramagnetic +1 state can be ruled out. In fact, optimization of $Au_{25}(SCH_3)_{18}^{+}$ in the triplet configuration gives an energy of 0.36 eV above that of the singlet. This result is thus consistent with our previous NMR[4] and current EPR measurements which show no paramagnetic behavior (in contrast to the strong paramagnetic behavior of the neutral state).[4,5] Note that while in the +1 state the $2a_u$ now becomes the LUMO, the $1a_u \rightarrow 2a_u$ transition is symmetry forbidden. Thus, the experimentally measured gap in the +1 case actually corresponds to the $1a_u/a_g$ gap. The calculated increase in this gap is 0.13 eV, again in good agreement with the experimental HOMO−LUMO gap measured from the UV−vis absorption onset data (0.2 eV). Notice that the observation of a severe splitting in the HOMO manifold in the +1 species, consistent with our EPR results, does not support a recent interpretation of thermal stability based on a superatom picture.[42] Thus, we suggest that a superatom model representation for the diradical cation species is inadequate.

The optical absorption spectrum was also computed for the −1, 0, and +1 charge states at the TDDFT level of theory. In the strict sense, these calculations correspond to zero temperature. This observation is relevant because it has been shown that the optical absorption properties of Au_{25} and Au_{38} clusters display a strong dependency on temperature.[43] Figure 10 shows that all charge states have a double peak structure for the excitations involving $1a_u \rightarrow a_g$ transitions. As Figure 8 shows, such splitting originates from transitions starting from the two different levels in the $1a_u$ manifold (i.e., HOMO → LUMO and HOMO-1 → LUMO). Whereas these peaks are much less resolved in the experimental spectra obtained at 298 K,[4,9] Devadas et al. have shown that these features are completely resolved at 78 K for $Au_{25}(SC_6H_{13})_{18}^{-}$:[43] the two peaks are located at 1.67 and 1.9 eV, with the second peak 1.5 times higher than the first. Our calculations give two peaks at 1.47 and 1.61 eV, with the second peak 1.2 times higher than the first. Note that this level of agreement on the absolute values of the peak positions is typical in TDDFT calculations for this type of systems.[6c,d,7]

In summary, all the results shown here are consistent with the conclusions drawn by EPR, NMR, and UV−vis, confirming the accuracy of our DFT calculations. Of special relevance is the finding that a triplet state for $Au_{25}(SR)_{18}^{+}$ nanoparticles would be inaccessible for a large range of temperatures. Therefore, $Au_{25}(SR)_{18}^{+}$ exhibits, unambiguously, a diamagnetic character.

CONCLUSIONS

$Au_{25}(SR)_{18}$ is often taken as an example of a well-understood cluster.[1b] On the other hand, very recent research is also providing quite unclear or even controversial description of its properties. In the search of a self-consistent picture, we prepared highly pure, monodisperse $Au_{25}(SR)_{18}^{0}$ clusters and studied their electrochemical and EPR behaviors under precisely controlled conditions. CV was employed to assess the kinetics of $Au_{25}(SR)_{18}^{0}$ reduction, to form the −1 and −2 charge states, and oxidation, to form the +1, +2, and +3 charge states. Formation of all charged species is endowed by inner-reorganization energy 4−5 times larger than the solvent reorganization energy, i.e., the opposite of what happens with common delocalized ion radical species in organic solvents.[31] As opposed to the stable −1, 0, and +1 charge states, $Au_{25}(SR)_{18}^{2-}$, $Au_{25}(SR)_{18}^{2+}$, and $Au_{25}(SR)_{18}^{3+}$ are labile species with lifetimes of 4 ms, 0.33 s, and 20 ms, respectively. These results clearly demonstrate that the interpretations of recent optical measurements[14] and electrochemical results involving one or more of these species[18] need to be re-examined very carefully.

The three HOMOs of $Au_{25}(SR)_{18}$ are consistently depicted as degenerated or almost degenerate.[6] By taking into account the EPR[5] and NMR evidence[4] that $Au_{25}(SR)_{18}^{0}$ is paramagnetic, one is tempted to assume that $Au_{25}(SR)_{18}^{+}$ should be a triplet. In fact, room temperature ^{1}H and ^{13}C NMR spectra indicate that the latter is diamagnetic,[4] but very recent EPR results pointed to $Au_{25}(SR)_{18}^{+}$ as having a distinct radical character.[11] However, the cw-EPR spectra of $Au_{25}(SR)_{18}^{+}$ reveal that the latter is not EPR active in the temperature range 6−260 K. The spectra of $Au_{25}(SR)_{18}^{0}$ were simulated using not only the same parameters described by Zhu et al[5] but also a

dx.doi.org/10.1021/ja407887d | J. Am. Chem. Soc. 2013, 135, 15585−15594

much smaller number of gold atoms, which shows that in this respect there is no need to invoke an Au_{13} superatom model. As opposed to commonly accepted views (i.e., HOMO levels remaining unaltered across charged species), our EPR study provides definite evidence that $Au_{25}(SR)_{18}^{+}$ is a diamagnetic species, i.e., has a ground state with two electrons low-spin paired (singlet state). Together with the NMR results obtained at 298 K,[4] the outcome of this study also indicates that the energy difference between the first and the second HOMO must be at least large enough to prevent formation of a triplet state at all temperatures investigated. Calculations confirm that such formation is energetically prohibitive.

We have shown that the DFT-computed optical absorption spectra and DOS of the −1, 0, and +1 charge states nicely reproduce the experimentally estimated dependence of the HOMO−LUMO energy gap on the actual charge carried by the cluster. DFT calculations provide a clear picture of the evolution of the frontier orbitals, confirming that the +1 charge state must be considered diamagnetic due to a significant splitting of the HOMO energy levels.

■ ASSOCIATED CONTENT

Supporting Information

Further details and figures about electrochemistry, EPR, and DFT structures' coordinates. This material is available free of charge via the Internet at http://pubs.acs.org.

■ AUTHOR INFORMATION

Corresponding Authors

flavio.maran@unipd.it

jose.gascon@uconn.edu

Notes

The authors declare no competing financial interest.

■ ACKNOWLEDGMENTS

This work was financially supported by the Italian Ministry of Education, University and Research (PRIN 20098Z4M5E), the University of Padova (PRAT CPDA103389). J.A.G acknowledges financial support from the NSF for a CAREER Award (CHE-0847340).

■ REFERENCES

(1) (a) Murray, R. W. *Chem. Rev.* **2008**, *108*, 2688−2720. (b) Parker, J. F.; Fields-Zinna, C. A.; Murray, R. W. *Acc. Chem. Res.* **2010**, *43*, 1289−1296.

(2) (a) Heaven, M. W.; Dass, A.; White, P. S.; Holt, K. M.; Murray, R. W. *J. Am. Chem. Soc.* **2008**, *130*, 3754−3755. (b) Zhu, M.; Aikens, C. M.; Hollander, F. J.; Schatz, G. C.; Jin, R. *J. Am. Chem. Soc.* **2008**, *130*, 5883−5885. (c) Zhu, M.; Eckenhoff, W. T.; Pintauer, T.; Jin, R. *J. Phys. Chem. C* **2008**, *112*, 14221−14224.

(3) (a) Negishi, Y.; Nobusada, K.; Tsukuda, T. *J. Am. Chem. Soc.* **2005**, *127*, 5261−5270. (b) Tracy, J. B.; Kalyuzhny, G.; Crowe, M. C.; Balasubramanian, R.; Choi, J.-P.; Murray, R. W. *J. Am. Chem. Soc.* **2007**, *129*, 6706−6707.

(4) Venzo, A.; Antonello, S.; Gascón, J. A.; Guryanov, I.; Leapman, R. D.; Perera, N. V.; Sousa, A.; Zamuner, M.; Zanella, A.; Maran, F. *Anal. Chem.* **2011**, *83*, 6355−6362.

(5) Zhu, M.; Aikens, C. M.; Hendrich, M. P.; Gupta, R.; Qian, H.; Schatz, G. C.; Jin, R. *J. Am. Chem. Soc.* **2009**, *131*, 2490−2492.

(6) (a) Akola, J.; Walter, M.; Whetten, R. L.; Häkkinen, H.; Grönbeck, H. *J. Am. Chem. Soc.* **2008**, *130*, 3756−3757. (b) Aikens, C. M. *J. Phys. Chem. C* **2008**, *112*, 19797−19800. (c) Aikens, C. M. *J. Phys. Chem. A* **2009**, *113*, 10811−10817. (d) Aikens, C. M. *J. Phys. Chem. Lett.* **2011**, *2*, 99−104.

(7) Aikens, C. M. *J. Phys. Chem. Lett.* **2010**, *1*, 2594−2599.

(8) Antonello, S.; Maran, F. *Chem. Soc. Rev.* **2005**, *34*, 418−428.

(9) Antonello, S.; Hesari, M.; Polo, F.; Maran, F. *Nanoscale* **2012**, *4*, 5333−5342.

(10) Liu, Z.; Zhu, M.-Z.; Meng, X.; Xu, G.; Jin, R. *J. Phys. Chem. Lett.* **2011**, *2*, 2104−2109.

(11) Arash Akbari-Sharbaf, A.; Hesari, M.; Workentin, M. S.; Fanchini, G. *J. Chem. Phys.* **2013**, *138*, 024305−1−024305−5.

(12) Lee, D.; Donkers, R. L.; Wang, G.; Harper, A. S.; Murray, R. W. *J. Am. Chem. Soc.* **2004**, *126*, 6193−6199.

(13) Antonello, S.; Holm, A. H.; Instuli, E.; Maran, F. *J. Am. Chem. Soc.* **2007**, *129*, 9836−9837.

(14) Wu, Z.; Jin, R. *Nano Lett.* **2010**, *10*, 2568−2573.

(15) Marcus, R. A.; Sutin, N. *Biochim. Biophys. Acta* **1985**, *811*, 265−322.

(16) Parker, J. F.; Choi, J.-P.; Wang, W.; Murray, R. W. *J. Phys. Chem. C* **2008**, *112*, 13976−13981.

(17) Choi, J.-P.; Murray, R. W. *J. Am. Chem. Soc.* **2006**, *128*, 10496−10502.

(18) (a) Fang, Y.-M.; Song, J.; Li, J.; Wang, Y.-W.; Yang, H.-H.; Sun, J.-J.; Chen, G.-N. *Chem. Commun.* **2011**, *47*, 2369−2371. (b) Swanick, K. N.; Hesari, M.; Workentin, M. S.; Ding, Z. *J. Am. Chem. Soc.* **2012**, *134*, 15205−15208.

(19) Antonello, S.; Musumeci, M.; Wayner, D. D. M.; Maran, F. *J. Am. Chem. Soc.* **1997**, *119*, 9541−9549.

(20) Meneses, A. B.; Antonello, S.; Arévalo, M.-C; Maran, F. *Electroanalysis* **2006**, *18*, 363−370.

(21) See: Clegg, A. D.; Rees, N. V.; Klymenko, O. V.; Coles, B. A.; Compton, R. G. *J. Electroanal. Chem.* **2005**, *580*, 78−86 and references therein.

(22) Nicholson, R. S. *Anal. Chem.* **1965**, *37*, 1351−1355.

(23) Ahlrichs, R.; Bär, M.; Häser, M.; Horn, H.; Kölmel, C. *Chem. Phys. Lett.* **1989**, *162*, 165−169.

(24) Stoll, S.; Schweiger, A. *J. Magn. Reson.* **2006**, *178*, 42−55.

(25) Nicholson, R. S.; Shain, I. *Anal. Chem.* **1964**, *36*, 706−723.

(26) The *D* and rate constant values have been recalculated with respect to the previously reported values,[13] which were affected by the wrong stoichiometry previously assigned to Au_{25}.[1]

(27) Holm, A. H.; Ceccato, M.; Donkers, R. L.; Fabris, L.; Pace, G.; Maran, F. *Langmuir* **2006**, *22*, 10584−10589.

(28) Bard, A. J.; Faulkner, L. R. *Electrochemical Methods, Fundamentals and Applications*, 2nd ed.; Wiley: New York, 2001.

(29) Owing to the change in the *D* value,[26] these k° values slightly differ from previously reported results, obtained starting from $Au_{25}(SR)_{18}^{-}$ instead of $Au_{25}(SR)_{18}$.[0,13]

(30) Kojima, H.; Bard, A. J. *J. Am. Chem. Soc.* **1975**, *97*, 6317−6324.

(31) Meneses, A. B.; Antonello, S.; Arévalo, M. C.; González, C. C.; Sharma, J.; Wallette, A. N.; Workentin, M. S.; Maran, F. *Chem.—Eur. J.* **2007**, *13*, 7983−7995.

(32) Antonello, S.; Maran, F. *J. Am. Chem. Soc.* **1999**, *121*, 9668−9676.

(33) Hush, N. S. *Electrochim. Acta* **1968**, *13*, 1005−1023.

(34) Vericat, C.; Vela, M. E.; Benitez, G.; Carro, P.; Salvarezza, R. C. *Chem. Soc. Rev.* **2010**, *39*, 1805−1834.

(35) Walter, M.; Akola, J.; Lopez-Acevedo, O.; Jadzinsky, P. D.; Calero, G.; Ackerson, C. J.; Whetten, R. L.; Grönbeck, H.; Häkkinen, H. *Proc. Natl. Acad. Sci. U.S.A.* **2008**, *105*, 9157−9162.

(36) Chateauneuf, J.; Lusztyk, J.; Ingold, K. U. *J. Am. Chem. Soc.* **1988**, *110*, 2886−2893.

(37) For the Curie law see, for example: Carlin, R. L.; *Magnetochemistry*, Springer-Verlag: Berlin, Heidelberg, Germany, 1986, pp 5−11. Interestingly, the plot of the EPR intensities (I_{EPR}) obtained from the double integration of the EPR spectra of Figure 7 (see caption) as a function of $1/T$ is quite linear (Figure S5 of SI). From the basic theory of EPR spectroscopy, the power P_a absorbed by the magnetic system from the microwave field (B_1) depends linearly on the static magnetic susceptibility χ_0 (see eq. 10.31, Chapter 10, of ref 40a). According to the Curie law (valid for paramagnetic diluted systems), χ_0 follows a linear trend with respect to $1/T$ and, therefore, also the

adsorbed power P_a depends linearly on $1/T$. This is indeed a very unusual behavior for a nanoparticle[37a] that, however, could be related to the effective molecule-like properties of $Au_{25}(SR)_{18}^0$. (a) Nealon, G. L.; Donnio, B.; Greget, R.; Kappler, J.-P.; Terazzi, E.; Gallani, J.-L. *Nanoscale* **2012**, *4*, 5244−5258.

(38) The large line width values provided by the simulations (caption to Figure 7) can be accounted for by the inhomogeneous broadening that primarily occurs in EPR lines due to unresolved hyperfine components.

(39) For a survey of the theory about *g*-tensor and ZFS, see for instance: Bennati, , M.; Murphy, , D. M. . In *Electron Paramagnetic Resonance − A Practioner's Toolkit*; Brustolon, , M., Giamello, , E.; Eds.; John Wiley & Sons, Inc.: Hoboken, New Jersey, **2009**,, pp 195−−238.

(40) (a) Weil, J. A.; Bolton, J. R.; Wertz, J. E. *Electron Paramagnetic Resonance − Elementary Theory and Practical Applications*; John Wiley & Sons, Inc.: Hoboken, New Jersey, 1994, pp 287−333. (b) Pilbrow, J. R. *Transition Ion Electron Paramagnetic Resonance*; Clarendon Press: Oxford, 1990, pp 368−394. (c) Slichter, C. P. *Principles of Magnetic Resonance*; Springer: New York, NY, 1990, pp 11−64. (d) Fraenkel, G. K. *J. Phys. Chem.* **1967**, *71*, 139−171.

(41) In general, for non-negligible ZFS or in the presence of *g*-factor anisotropies, the standard Bloch formalism for describing relaxation is not adequate and a more advanced density-matrix theory is required: (a) Lynden-Bell, R. M. The Calculation of Lineshapes by Density Matrix Methods. In *Progress in NMR Spectroscopy*; Emsley, J. W., Feeney, J., Sutcliffe, L. H.; Eds.; Pergamon Press, London, 1967, Chapter 2. (b) Binsch, G. The Study of Intramolecular Rate Processes by Dynamic Nuclear Magnetic Resonance. In *Topics in Stereochemistry*, Eliel, E. L., Allinger, N. L., Eds.; Wiley-Interscience: New York, 1968; Vol. 3, pp 97−192.

(42) Tofanelli, M. A.; Ackerson, C. J. *J. Am. Chem. Soc.* **2012**, *134*, 16937−16940.

(43) Devadas, M. S.; Bairu, S.; Qian, H.; Sinn, E.; Jin, R.; Ramakrishna, G. *J. Phys. Chem. Lett.* **2011**, *2*, 2752−2758.